Catalysis Letters (2024) 154:1094–1111
https://doi.org/10.1007/s10562-023-04370-7

Zirconia Incorporated Aluminum Phosphate Molecular Sieves as Efficient Microporous Nano Catalysts for the Selective Dehydration of Methanol into Dimethyl Ether

Abd El-Aziz Ahmed Said[1] · Aya Ali Shaban[1] · Mohamed Nady Goda[1]

Received: 22 January 2023 / Accepted: 14 May 2023 / Published online: 2 June 2023

Abstract
Annually, a growing demand was noted for replacing petroleum fuels with second-generation eco-friendly fuels like dimethyl ether (DME). Methanol dehydration into DME process has been considered as one of the potential pathways for the manufacture of a clean fuel. However, stable, and active catalyst is exceedingly requisite for generation of DME particularly at reasonably low temperature. In the current study, zirconia incorporated $AlPO_4$ tridymite microporous molecular sieve catalysts were fabricated by a hydrothermal method in the presence of triethylamine (TEA) as a structure directing agent. The catalysts were characterized by X-ray diffraction (XRD), energy dispersive X-ray (EDX), Fourier transform infrared spectroscopy (FTIR), transmission electron microscopy (TEM), thermogravimetric analysis (TGA), and N_2-sorption assessments. Catalysts' acidity was estimated by decomposition of isopropanol, pyridine and dimethyl pyridine chemisorption, and pyridine-TPD. Results revealed that catalysts surfaces composed acid sites of Brønsted nature and of weak and medium strengths. Activity results showed that 1 wt% H_2SO_4 modified zirconia incorporated $AlPO_4$-TRI catalyst calcined at 400 °C presented the best activity with a conversion of 89% and a 100% selectivity into DME at 250 °C. The significant catalytic activity is well-connected to the variation in BET-surface area, acidity, and activation energy of methanol dehydration. The catalysts offered long-term stability for 120 h and could be regenerated with almost the same activity and selectivity.

✉ Abd El-Aziz Ahmed Said
a.a.said@aun.edu.eg

[1] Catalysis and Surface Chemistry Lab, Department of Chemistry, Faculty of Science, Assiut University, Assiut 71516, Egypt

Graphical Abstract

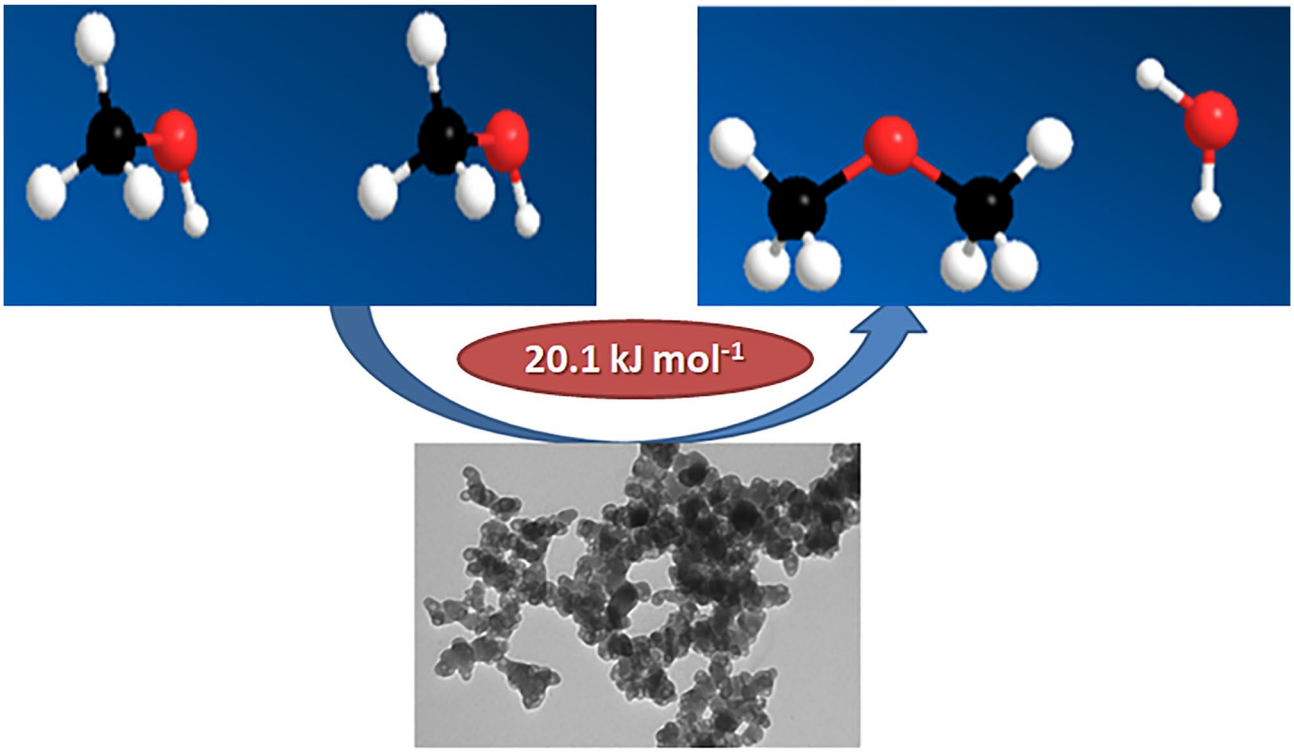

Keywords Dimethyl ether · Acidity · Characterization · Fuel

1 Introduction

Air contaminants such as NO_x, SO_x and particulates, which are exhausted from the on-board diesel engines of buses and trucks, are considered one of the most serious environmental problems all over the world. Thus, there is a continuously emergent demand for new and clean energy sources to replace the air-polluting sources, and to replenish the growth in the global energy expenditure and the reduction in current energy sources. Among the numerous sources of energy, DME has been viewed as a second-generation energy source that may soon replace petroleum fuels as a crucial chemical feedstock [1]. Owing to its high cetane number (55–60), high energy density (31.7 MJ kg^{-1}), low particulate matter emissions, and smoke-free emissions compared with traditional diesel fuels [2, 3], DME has been acknowledged as an alternative fuel for the compression–ignition machines. In addition, it serves as a great supply of H_2 for the catalytic steam reforming process and is non-toxic, non-carcinogenic, non-corrosive, and non-mutagenic [4]. Moreover, DME is used as an effective intermediate compound in production of several chemicals and as an aerosol propellant such as shaving cream, and hair spray, to substitute the ozone-destroying chlorofluorocarbons (CFCs). According to these benefits, by 2026 its production is expected to reach 5867.28 ktons [5].

DME can be produced via two processes [6–9]: methanol dehydration over solid acid catalyst that is usually pure or modified γ-Al_2O_3 (Eq. 1) [7] and direct synthesis from syngas over bifunctional catalyst containing metal oxide and solid acid catalysts [9–11] (Eq. 2).

$$2CH_3OH \rightarrow CH_3OCH_3 + H_2O, \quad (1)$$

$$3CO + 3H_2 \rightarrow CH_3OCH_3 + CO_2. \quad (2)$$

From thermodynamics and economic points of views, a methanol-to-dimethyl ether (MTD) is favorable and is a one-step reaction with high efficiency in comparison with the other methods [10–12]. This process, i.e. MTD, is first used in a fixed bed reactor by Mobil 1965 [13] and further applied by various organizations such as Uhde, Lurgi, and Toyo. However, numerous catalysts were reported for MTD process including zeolites [14–17], γ-Al_2O_3 [15, 18], heteropoly acids [19, 20], sulphonated SiO_2 and MCM-41 [21], $ZrOSO_4$@C [6], ZrO_2–$FePO_4$ [22], Nb_2O_5–Al_2O_3

[23], SO_4^{2-}–ZrO_2 [24] and SAPO-11 [25] in a temperature range of 250–400 °C. However, these materials displayed high catalytic activity compared to the most frequently used γ-Al_2O_3, but they are less resistive to be deactivated than γ-alumina. The presence of strong acid sites on the surface of γ-Al_2O_3 is reason for the creation of side products such as olefins and coke formation [26]. In addition, water molecules are adsorbed on the strong Lewis acid sites over γ-Al_2O_3, resulting in a decrease in the quantity of active acidic sites which ultimately leading to a decay in the catalytic activity of γ-Al_2O_3 [27]. To prevent such non-desired reaction products, such olefins and coke, and improve the selectivity to the DME, a solid acid catalyst of weak or moderate Brønsted acidity is desirable [28, 29]. It is apparent that the choice of a proper catalyst for methanol dehydration is determined on several factors including nature and strength of acidic sites, morphology and its texture properties, active temperature range and resistance, harmfulness, and its deactivation. These aspects must be considered in terms of the cost-effectiveness of a given catalytic material. Thus, it is of an essential concern to find an efficient, selective, and durable catalyst with a suitable acidity for MTD with high conversion and 100% selectivity.

Aluminophosphate zeolite are important and large family of molecular sieves of large pores, uncharged framework and excellent thermal stability [30]. Due to their silica-free composition, aluminum phosphate molecular sieves, a class of similar zeolite frameworks, have garnered considerable study interest. However, because of their structural similarities to those of regular zeolite, these unique materials have a great deal of potential for use in a wide range of applications, including adsorption, catalytic processes, and separation membranes [31]. Their frameworks consist of alternate oxygen-sharing AlO_4 and PO_4 tetrahedral. Through the use of structure-directing agents (SDAs) during hydrothermal crystallisation, recent advancements in experimental syntheses have made it possible to regulate the distribution and arrangement of the Al^{3+} framework [32, 33]. Their characteristics may be altered by substituting Al^{3+} or P^{5+} in the framework with appropriate elements, resulting in the development of exchanged molecular sieves [34]. Accordingly, metal ions could be successfully incorporated into aluminophosphate molecular sieves. Zirconium is a transition metal that has catalytic characteristics, particularly in oxidation reactions [35, 36]. As sensible from literature, a group of researchers synthesized aluminophosphate zeolite (AlPO-5), characterization, and exploring their applications. In this concern, Sajan et al. [37] confirmed the synthesis of AlPO-5 by XRD studies, FTIR, and SEM, and studied its application for treatment of wastewater and industrial effluents. According to Said et al. [31], $AlPO_4$-5 was the active catalyst for diethyl ether (DEE) synthesis with a conversion of 81.5%, owing to its lower acidity and strength density. Meanwhile, Mo–Zn/$AlPO_4$-5 was the most selective for ethylene formation (93%), owing to the increase in acid site density, which favored ethylene generation [31]. Mortén et al. [38] studied the isomorphous substitution of AlPO-5 materials with Mg, Zn, Co, Si, Ti, and Zr. They reported that Zr has led to catalysts with the same AFI structure but significantly different acid strengths, and a correlation of the influence of acidity on the methylation of benzene was investigated. Dongare et al. [39] implied that Zr was isomorphously replaced in the AlPO-5 structure. They found that, an enhancement was observed in activity and stability towards the *m*-xylene isomerization process owing to the enhancement in both Brønsted and Lewis acidity.

However, keeping in mind the catalytic activity of the microporous aluminophosphate mentioned above, little reports were seen in literature concerning the use of zeolitic aluminum phosphate like AlPO-5, AlPO-11 and AlPO-41 for methanol dehydration into DME [40]. In these reports, despite the high conversion (81–82.4%) and DME selectivity (99.6%), the reaction operated at relatively high temperatures of 350 °C. Accordingly, the main object of the current work was the selective production of DME from methyl alcohol dehydration over pure and Zr incorporated aluminophosphate microporous catalysts at comparatively low temperatures than previously reported in literature. Characterization techniques such as XRD, EDX, HRTEM, FTIR, and TG were employed. Acidity measurements were carried out and well linked with the catalytic activity. The impact of different operational factors was also examined. $AlPO_4$-TRI in this study were proved as efficient catalysts for producing DME from methanol dehydration with high conversion, and 100% selectivity.

2 Experimental

2.1 Materials

Aluminum chloride anhydrous (BDH, England), diammonium hydrogen orthophosphate [Alfa Aesar (98%)], zirconium oxychloride octahydrate (Alfa Aesar, 98%), and triethylamine (BDH) were chosen as the starting materials in the synthesis of pure and Zr-incorporated $AlPO_4$-tridymite microporous molecular sieves. Methanol (CH_3OH, 99.6%), isopropyl alcohol (IPA, $CH_3CHOHCH_3$, 99.5%), pyridine (C_5H_5N, 99.5%), sulfuric acid (BDH, England) and 2, 6-dimethyl pyridine (C_7H_9N, 99.9%) were provided as pure reagents.

2.2 Catalyst Preparation

Aluminophosphate ($AlPO_4$-TRI) molecular sieves were prepared adopting the hydrothermal method as previously

reported with some modifications [37, 41]. This method includes a regulated co-polymerization and co-precipitation of aluminate and phosphate in a homogeneous gel phase. In a typical synthesis of $AlPO_4$-TRI with a general formula of Al_2O_3:P_2O_5:TEA:80 H_2O, an 8.20 mmol of trimethylamine (TEA) was added to an 8.20 mmol of aluminum chloride dissolved in 50 ml of distilled water. The produced precursor gel was aged for 15 min at 50 °C. To this mixture, an 8.20 mmol of ammonium hydrogen orthophosphate was added and stirred for 30 min to get a uniform gel. The as-prepared aluminophosphate gel was poured into a Teflon-lined autoclave (polytetrafluoroethylene) and heated for 24 h at 160 °C. After the experimental treatment was completed, the autoclave was quenched out and the product was filtered, washed thoroughly using bidistilled water and dried for 24 h at 80 °C before annealing at 400 °C. The other catalysts composing various ratios of structure directing agent to Al (Al/TEA) were prepared by the same manner and designed as $AlPO_4$-0.8T, $AlPO_4$-1.2T, and $AlPO_4$-1.4T.

To synthesis a Zr incorporated $AlPO_4$-TRI with a general formula of $xZrO_2$:$(1-x)Al_2O_3$:P_2O_5:TEA:80 H_2O [41], the same procedures were used as above with introduction of $ZrOCl_2 \cdot 8H_2O$ in the preparation steps. x Values in these catalysts were varied from 0.05 to 0.5 as 0.05, 0.1 0.3, 0.5. The most effective catalyst, as determined by the catalytic activity runs, was $AlPO_4$-TRI incorporated with Zr of $x = 0.1$. Consequently, it was selected as a representative catalyst to study the influence of modification with different ratios of sulfuric acid (0.5%, 1%, 3%, 5%). These catalysts were prepared using the impregnation method. Table 1 describes the detailed nomenclature for each abbreviation.

2.3 Catalyst Characterization

The crystal structure of the prepared nanocatalysts were identified by a PW 2013 Philips diffractometer ($\lambda = 1.5418$ Å, 200 mA, and 35 kV) using Cu Kα radiation, and nickel filtered. The different functional groups were detected with a 6700 Nicolet FTIR spectrophotometer in 400–4000 cm^{-1} range at room temperature and the disc was prepared at a pressure of 10 tons. A Quantachrome NOVA (model 3200, USA) was used to evaluate the texture using N_2 adsorption–desorption analysis at − 196 °C. A JSM-5400 LV microscope (JEOL, Tokyo, Japan) were used to investigate the morphological properties of the catalysts. EDX analysis for the investigated materials were obtained using SEM equipment (LEO 440 model). The samples were distributed in alcohol using an ultrasonication technique. A carbon-coated copper grid was then immersed with a few drops from the suspended solution, followed by solvent evaporation drying. Thermogravimetry (TG) was performed on an 50H thermal analyzer (TA-50WSI, Shimadzu, Japan) in air atmosphere (30 ml min^{-1}).

2.4 Acidity Evaluation

The acidic properties of the pure and Zr-incorporated $AlPO_4$-TRI catalysts were performed using IPA dehydration, pyridine, and 2, 6-dimethyl pyridine chemisorption, as previously described [22, 42, 43]. The conditional parameters were a catalyst dose of 100 mg, IPA of 2.8%, nitrogen as a carrier of flowing rate of 50 ml min^{-1}, and a temperature of 200 °C. An England Pye-Unicam ProGC gas chromatograph connected with a flame ionization detector (FID) and a 10% PEG 400 glass column (2 m) was utilized to follow the reaction and identify the products.

2.5 Catalytic Activity Test

The catalytic behavior of these catalysts towards DME production was investigated as reported elsewhere [44, 45]. The reaction conditions included using nitrogen as a carrier gas, 200 mg of catalyst, and 4.6% methanol in a stream of N_2 gas flowing at a total flow rate of 50 ml min^{-1}.

Table 1 Nomenclature of the synthesized catalysts

Abbreviation	Catalyst
$AlPO_4$-0.8T	Al:P 1:1, Al:TEA 1:0.8
$AlPO_4$-1T	Al:P 1:1, Al:TEA 1:1
$AlPO_4$-1.2T	Al:P 1:1, Al:TEA 1:1.2
$AlPO_4$-1.4T	Al:P 1:1, Al:TEA 1:1.4
0.05Zr-$AlPO_4$-1T	$0.05ZrO_2$:$0.95Al_2O_3$:P_2O_5:TEA:$80H_2O$
0.1Zr-$AlPO_4$-1T	$0.1ZrO_2$:$0.9Al_2O_3$:P_2O_5:TEA:$80H_2O$
0.3Zr-$AlPO_4$-1T	$0.3ZrO_2$:$0.7Al_2O_3$:P_2O_5:TEA:$80H_2O$
0.5Zr-$AlPO_4$-1T	$0.5ZrO_2$:$0.5Al_2O_3$:P_2O_5:TEA:$80H_2O$
0.5% H_2SO_4–0.1Zr-$AlPO_4$-1T	($0.1ZrO_2$:$0.9Al_2O_3$:P_2O_5:TEA:$80H_2O$) modified with 0.5% H_2SO_4
1% H_2SO_4–0.1Zr-$AlPO_4$-1T	($0.1ZrO_2$:$0.9Al_2O_3$:P_2O_5:TEA:$80H_2O$) modified with 1% H_2SO_4
3% H_2SO_4–0.1Zr-$AlPO_4$-1T	($0.1ZrO_2$:$0.9Al_2O_3$:P_2O_5:TEA:$80H_2O$) modified with 3% H_2SO_4
5% H_2SO_4–0.1Zr-$AlPO_4$-1T	($0.1ZrO_2$:$0.9Al_2O_3$:P_2O_5:TEA:$80H_2O$) modified with 5% H_2SO_4

Typical experimental runs were examined in the range of 200–300 °C under atmospheric pressure. The gaseous reaction products were analyzed on an FID by using DNP glass column connected with a Pye-Unicam ProGC instrument (England). Carbon mass balances along the catalytic runs were close to 99.9%. The following equations were used to calculate the conversion, selectivity, and yield of DME over the surface of catalysts [6, 44]:

$$(\%)\ \text{Methanol conversion} = \frac{[\text{Methanol}]_{in} - [\text{Methanol}]_{out}}{[\text{Methanol}]_{in}} * 100, \quad (1)$$

$$(\%)\ \text{Selectivity to DME} = \frac{[\text{DME}]}{[\text{DME}] + [\text{Other products}]} * 100, \quad (2)$$

$$(\%)\ \text{Yield of DME} = (\text{Conversion} \times \text{Selectivity})/100, \quad (3)$$

where $[]_{in}$ and $[]_{out}$, respectively, refers to the amount of methyl alcohol in the inlet and exit stream.

The activation energy (ΔE_a) for methanol dehydration over pure and Zr-modified aluminophosphate catalysts was estimated using Arrhenius' equation, as described before [46, 47]. The initial rate (k) of methanol conversion was determined as the number of molecules that react each second per gram of catalyst using the formula: k = (C°X C X F)/m where C° is the starting methyl alcohol (molecule ml^{-1}), C is the conversion of methanol, F represents the reacting stream flow rate, and m is the mass of catalyst in grams. Plotting of ln k versus the reciprocal of absolute temperature (1/T) provides the calculation of ΔE_a.

3 Results and Discussion

3.1 Catalyst Characterization

3.1.1 X-ray Diffraction (XRD)

The powder X-ray diffractograms of aluminophosphate molecular sieves composing various ratios of TEA solids calcined at 400 °C are recorded and given in Fig. 1a. Results revealed that, the diffractograms of catalysts of TEA: Al of 0.8 and 1.0 are well-matched with the pure form of monoclinic $AlPO_4$-tridymite ($AlPO_4$-TRI) [41, 48] and JCPDS No. 36-735. In addition, the XRD patterns of the catalyst containing 1.0 TEA and the simulated card of monoclinic $AlPO_4$-tridymite is given in Fig. S1 which shows a complete agreement with the tridymite phase of aluminum phosphate. This phase is characteristic with strong diffractions at 2θ of 20.1°, 21.4°, and 22.9° which are clearly observed in our case (Fig. 1; Fig. S1). Results also revealed that a weak diffraction peak at 2θ of 26.5°, which corresponds to Berlinite phase. Increasing the ratio of the TEA into 1.2 and 1.4 ($AlPO_4$-1.2, and $AlPO_4$-1.4), resulted in converting the crystalline form into an amorphous structure with a hup at 2θ of 25.5°. The same behavior was observed on raising the calcination temperature of $AlPO_4$-1T above 400 °C (Fig. 1b). In addition, the particle size of $AlPO_4$-1T, and $AlPO_4$-0.8T catalysts calculated by the Scherrer's equation are approximately 18.7 nm and 21.9 respectively. Diffractogram of the 0.1Zr incorporated $AlPO_4$-1T catalyst is displayed in Fig. 1c. As illustrated, a broadening of the peaks was observed with a decrease in their intensity. Similar observations were previously reported [49, 50]. In addition, no other peaks corresponding to Zr were noted, reflecting the complete dissolution of Zr^{4+} in the molecular sieve's matrix. The Zr-incorporation was also confirmed by EDX analysis, as depicted in Table 1 in the forthcoming section. XRD diffractogram of 0.1Zr-$AlPO_4$-1T modified with 1 wt% H_2SO_4 is given in Fig. 1c. It exhibited the same diffractogram of 0.1Zr incorporated $AlPO_4$-1T.

3.1.2 Fourier Transform Infrared (FTIR)

Figure 2 shows the FTIR spectra of $AlPO_4$-1T (annealed at 400, 500, 600 °C), 0.1Zr-$AlPO_4$-1T and 1% H_2SO_4–Zr-$AlPO_4$-1T catalysts calcined at 400 °C. The strong absorption band in the region at about 1105 cm^{-1} is a special feature for the $AlPO_4$-1T molecular sieves containing hydrated triple crankshaft channels [37]. Such vibration in this region is due to the asymmetric stretching of PO_4 tetrahedral [51]. Another evidenced peaks corresponding to zeolite $AlPO_4$-TRI are the vibration bands at 640 and 475 cm^{-1}, which are attributed to the bending vibration modes of O–P–O and double ring respectively [37]. The peak centering at 1600 cm^{-1} corresponds to the bending vibration modes of water molecules or surface hydroxyl on the solid surface [52, 53]. The broadband positioned at 3505 cm^{-1} is due to the stretching mode of P–OH or Al–OH groups, which is proportional to catalyst acidity [54, 55]. As illustrated, its intensity increases with Zr^{4+} incorporation and sulfuric acid modification, reflecting the observable enhancement in the number of acidic sites due to the incorporation and impregnation processes [56]. Spectral vibrations also inferred that increasing the annealing temperature resulted in decreasing the intensities of peaks allocated at 3505 and 1600 cm^{-1} which leads to decreasing the catalysts' acidity.

3.1.3 Thermogravimetry (TG)

The thermal behavior of the pure and Zr-incorporated $AlPO_4$-1T molecular sieves precursors were examined using thermogravimetric analysis (TGA). Figure 3 shows the TG curves for $AlPO_4$-1T and 0.1Zr-$AlPO_4$-1T catalysts in air atmosphere. TG curve of the $AlPO_4$-1T exhibits three weight losses. The first weight loss of 11.5% was detected in the temperature range of 25–185 °C due to the

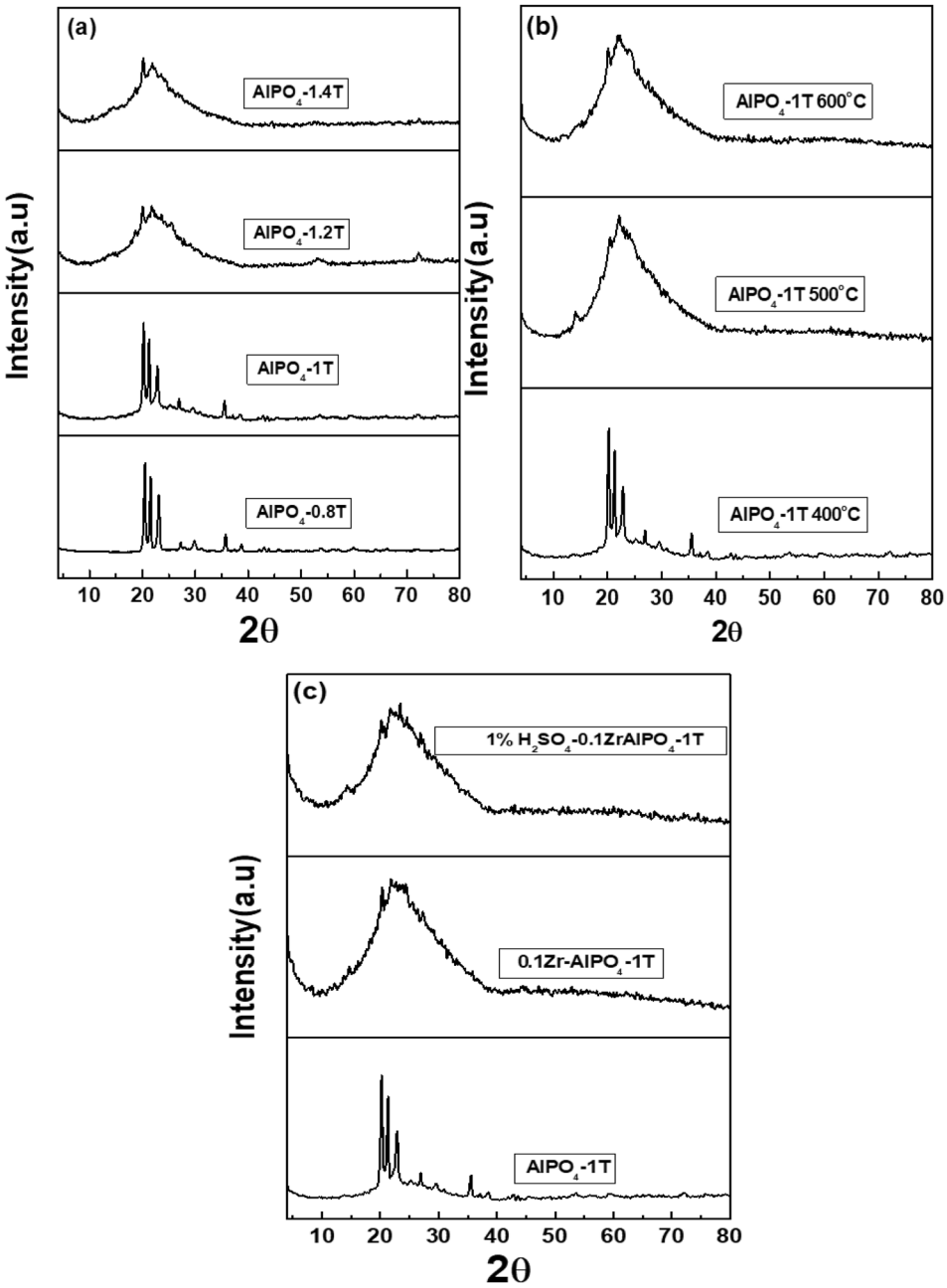

Fig. 1 X-ray diffractograms of **a** $AlPO_4$-TRI with different ratios Al/TEA catalysts calcined at 400 °C, **b** $AlPO_4$-1T calcined at different temperatures, and **c** pure and sulfuric acid modified 0.1Zr-$AlPO_4$-1T catalysts calcined at 400 °C

progression of adsorbed water molecules. The subsequent weight loss (5.5%) lies in the range of 186–249 °C and is linked to removal of water occluded in the molecular sieves. The third weight loss of 4.8% in the 250–324 °C range is attributed to removal of TEA [57, 58]. Other thermal changes on TG were not identified when the temperature was raised up to 600 °C, indicating that the produced $AlPO_4$-1T catalyst is thermally stable. The TG curve of the 0.1Zr-$AlPO_4$-1T catalyst exhibited a similar behavior as that of the $AlPO_4$-1T catalyst.

3.1.4 Electron Microscopy

TEM micrographs, and the corresponding particle size distribution histograms of $AlPO_4$-1T, and 0.1Zr-$AlPO_4$-1T catalysts calcined at 400 °C are given in Fig. 4. Micrographs revealed that the particles are uniformly distributed with spherical shape. The size of the $AlPO_4$-1T nanoparticles is about 20–30 nm (Fig. 4a), which is comparable with the results of Scherrer's equation. The particle size of 0.1Zr-$AlPO_4$-1T is around 15–20 nm, hence zirconia incorporation resulted in decreasing the particle sizes of pure

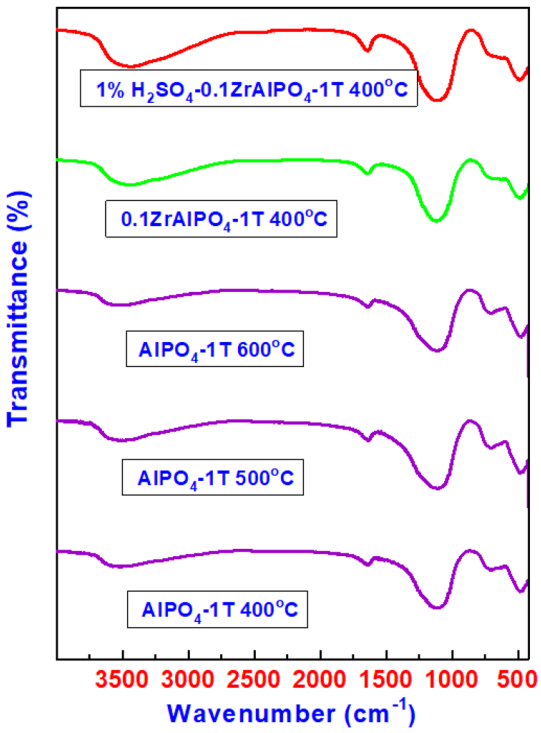

Fig. 2 FTIR spectra of $AlPO_4$-1T annealed at different temperatures, 0.1Zr-$AlPO_4$-1T, and 1% H_2SO_4/0.1Zr-$AlPO_4$-1T catalysts calcined at 400 °C

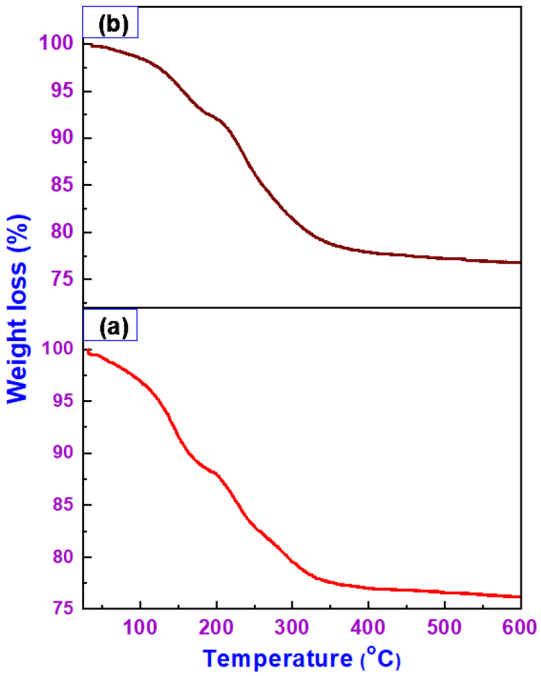

Fig. 3 TGA curves of **a** $AlPO_4$-1T, and **b** 0.1Zr-$AlPO_4$-1T precursors

$AlPO_4$-1T to be detected by XRD as shown from Fig. 1(c). In addition, ZrO_2 could not be detected from HRTEM reflecting the high distribution within the molecular sieve frameworks.

3.1.5 Energy Dispersive X-Ray (EDX)

The chemical analysis of the pure and Zr-substituted $AlPO_4$-1T was examined by EDX analysis and results are displayed in Fig. 5a, b and Table 2. EDX spectrum demonstrated the existence of Al, and P for $AlPO_4$-1T, while Al, P, and Zr elements were observed in Zr-$AlPO_4$-1T catalyst. It was previously reported that Al/P or (Al + Zr)/P ratio in aluminophosphate ideally should be close to unity [59]. Results presented in Table 1 confirmed this concept. Data also demonstrated that Al wt% in 0.1Zr-$AlPO_4$-1T decreases, confirming the substitution of Al by Zr species. All these findings confirmed the successful synthesis of both $AlPO_4$-1T and 0.1Zr-incorporated $AlPO_4$-1T. The atomic fractions of Al, P, and Zr were also evaluated by ICP. The fractions of Al, P, and Zr were 0.583, 0.417, and zero for the non-incorporated catalyst while, respectively, they are 0.579, 0.418, and 0.003% for the Zr-incorporated catalyst. The reason that the Al/P is higher than the unity, as predicted from the structure requirement, is the presence of some extra-framework of Al in the prepared catalysts [59].

3.1.6 Texture Assessment

The nitrogen adsorption–desorption isotherms of the pure and modified $AlPO_4$-1T materials are presented in Figs. S2–S5. All isotherms are of type II with little of type IV, which is typical of microporous materials [60]. These isotherms anchored to the type H4 hysteresis loop, which is often associated with narrows slit like pores. By using the BET equation in its typical application range ($p/p_o = 0.05–0.30$) with a cross-sectional area of $N_2 = 16.2$ Å^2, the specific surface areas, S_{BET}, of these catalysts were determined [22, 46]. The calculated S_{BET} values of catalysts are mentioned in Table 3. Results revealed that, on increasing the ratio of TEA from 0.8 to 1.0, an increase in the S_{BET} value from 35.8 to 48.4 $m^2\ g^{-1}$ was observed. The further raising of TEA:Al to 1.4 developed a drastic decrease in S_{BET} values to reach 19.8 $m^2\ g^{-1}$. On the other hand, the incorporation of Zr^{4+} into $AlPO_4$-1T matrix is accompanied by an increase in S_{BET} values where S_{BET} values increased from 48.4 into 125.5 $m^2\ g^{-1}$ on incorporating $AlPO_4$-1T matrix with a ratio of 0.3 mol% of Zr^{4+}. Also, the higher ratio of 0.5 mol% of Zr^{4+} leads to a decrease in S_{BET} value. Moreover, the influence of treatment of 0.1Zr-$AlPO_4$-1T with different percentages of H_2SO_4 on the texture properties was also investigated. Results indicated that impregnation with sulfuric acid also increases the value of S_{BET} to reach a maximum of 68.7 $m^2\ g^{-1}$ at 3% H_2SO_4, with an enhancement

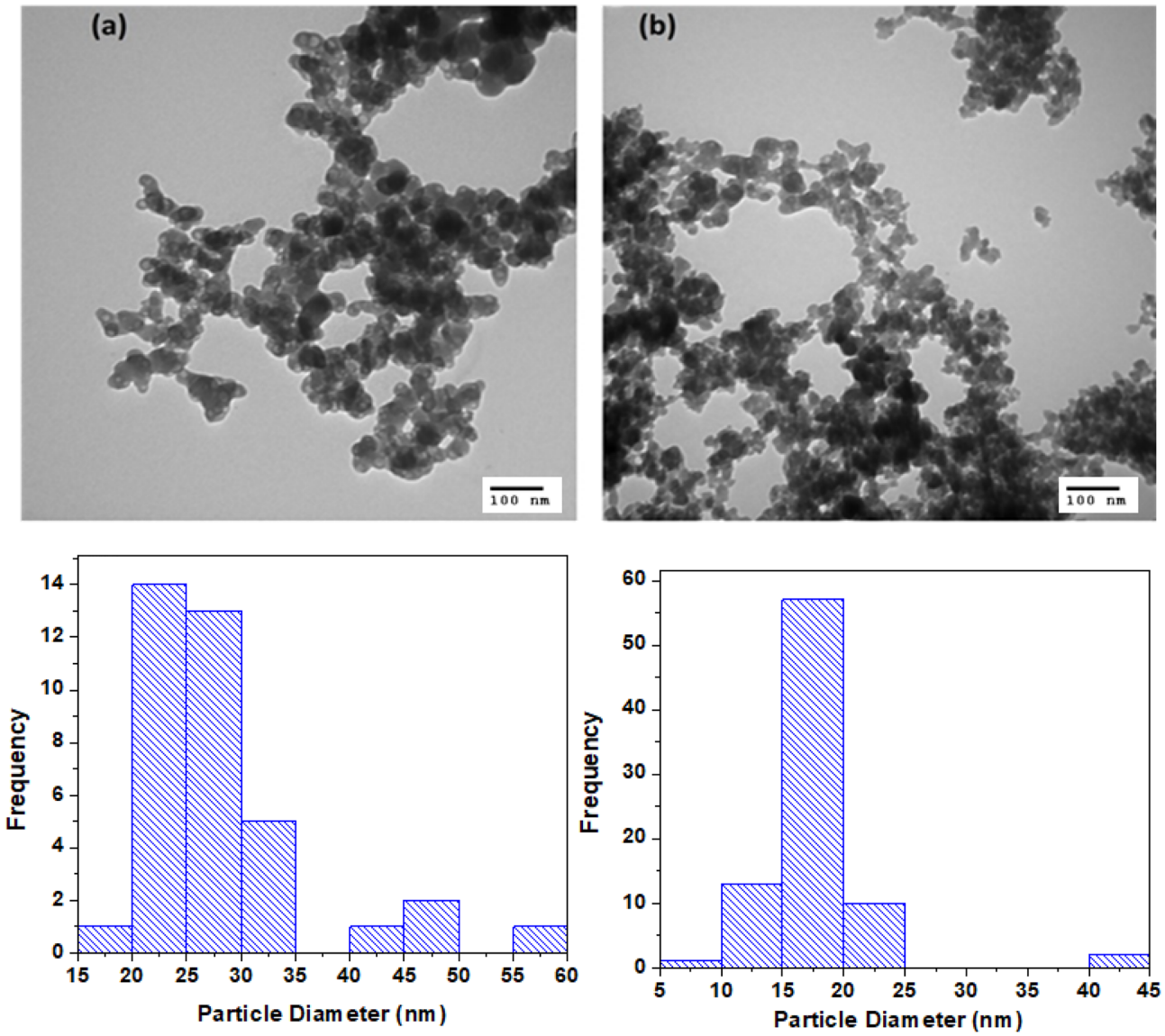

Fig. 4 TEM images and particle size distribution of **a** $AlPO_4$-1T, and **b** 0.1Zr-$AlPO_4$-1T catalysts calcined at 400 °C

in the values of S_{BET} by 24.3%. The enhancement observed in the S_{BET} values with TEA, Zr-incorporation and H_2SO_4 is well connected with the observable enhancement in the values of total pore volume (Table 3). Data recorded in Table 3 also showed that increasing the annealing temperature of $AlPO_4$-1T catalyst resulted in a decrease in S_{BET} values, which may be attributed to the sintering and blockage of pores [22].

To shed light on the microporosity presented by the catalysts under study, a BJH method is adopted, and the corresponding curves are graphically presented in Figs. S6–S9. In addition, the computed values of the average pore diameter were also cited in Table 3. It can be noted from the pore volume distribution curves for $AlPO_4$-1T with different additives of TEA (Fig. S6) that only one peak positioned at the value below 2 nm or 20 Å, indicating a microporous nature [46, 61]. Pore size distribution curves for $AlPO_4$-1T with 0.05 and 0.5 mol% of Zr^{4+} show one major peak placed at the value below 2 nm, together with a small peak in the mesopores region (2–50 nm or 20–500 Å, Fig. S8). This peak is shifted to the mesoporous zone for catalysts substituted with 0.1 and 0.3Zr. Pore size distribution curves of 0.1Zr-$AlPO_4$-1T impregnated with different ratios of sulfuric acid (Fig. S9) presented peaks in the microporous region, except that impregnated with 0.5% giving another peak in the mesopore region. These results indicate that the substitution with Zr^{4+} resulted in the creation of new mesopores while a microporous nature is still existing. The existence of microporosity was also confirmed from the values of average pore diameter cited in Table 3.

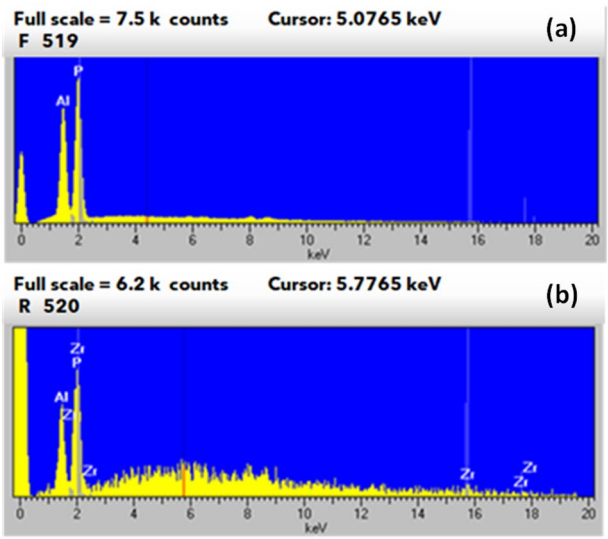

Fig. 5 EDX elemental mapping of **a** $AlPO_4$-1T, and **b** 0.1Zr-$AlPO_4$-1T catalysts calcined at 400 °C

Table 2 EDX analysis of pure and Zr-incorporated $AlPO_4$-1T catalysts

	$AlPO_4$-1T	0.1Zr-$AlPO_4$-1T
Al	11.5	10.4
P	11.2	11.7
Zr	–	0.8

Specific surface area (S_t) of the different catalysts could also be calculated from the t-method (Figs. S10–S13) using de-Bore method [22, 46] and the computed values were mentioned in Table 3. The variation in the S_t values exhibited the same trend observed in S_{BET} values. In addition, "both values of S_t and S_{BET} are closely spaced, indicating the correct choice of the standard t-curve". Moreover, the shape of V_a–t plot may reflect the nature of the present pores [62]. Figures S10–S13 show a downward deviation, which signifies a microporous nature of the pores and confirmed the results of pore size distribution method mentioned above [22, 46].

3.2 Acidity Measurements

Figure 6a displays the variation of IPA conversion as a function of reaction temperature over the representative catalyst 0.1 mol% Zr-$AlPO_4$-1T modified with 1% H_2SO_4. Results revealed that, within the reaction temperature range of 125–250 °C, the only product with a selectivity of 100% was propene, indicating that these catalysts' surfaces are acidic [6, 22, 63, 64]. In addition, IPA conversion increases with increasing of the reaction temperature to reach 100% at 250 °C. Figure 6b shows the variation of the % IPA conversion over $AlPO_4$-TRI with different ratios of TEA at 200 °C. It was found that values of IPA conversions of 25, 55, 22, 16% were obtained over catalysts with TEA/Al ratio of 0.8, 1.0, 1.2 and 1.4, respectively, reflecting that catalyst with equimolar ratio ($AlPO_4$-1T) exhibited the highest acidity.

Table 3 Texture properties of the different catalysts

Catalyst	S_{BET} ($m^2\ g^{-1}$)	S_t ($m^2\ g^{-1}$)	V_p ($cm^3\ g^{-1}$) 10^{-2}	Average pore diameter (Å)
$AlPO_4$-0.8T	35.8	35.7	3.9	15.9
$AlPO_4$-1T	48.4	48.3	5.3	15.5
$AlPO_4$-1.2T	22.8	22.9	1.6	15.8
$AlPO_4$-1.4T	19.8	19.6	2.3	15.9
0.05Zr-$AlPO_4$-1T	52.6	52.6	2.9	15.6
0.1Zr-$AlPO_4$-1T	55.3	55.3	9.3	15.8
0.3Zr-$AlPO_4$-1T	125.5	125.3	11.9	15.6
0.5Zr-$AlPO_4$-1T	98.3	98.1	7.2	17.5
$AlPO_4$-1T 500 °C	41.9	41.8	3.6	15.7
$AlPO_4$-1T 600 °C	30.0	30.1	2.3	15.9
0.5% H_2SO_4–0.1Zr-$AlPO_4$-1T	56.7	56.6	2.2	15.8
1% H_2SO_4–0.1Zr-$AlPO_4$-1T	63.3	63.3	8.5	15.7
3% H_2SO_4–0.1Zr-$AlPO_4$-1T	68.7	68.9	6.3	15.7
5% H_2SO_4–0.1Zr-$AlPO_4$-1T	47.8	47.6	4.9	18.1

V_p is total pore volume; average pore diameters were calculated from the desorption isotherm by BJH method

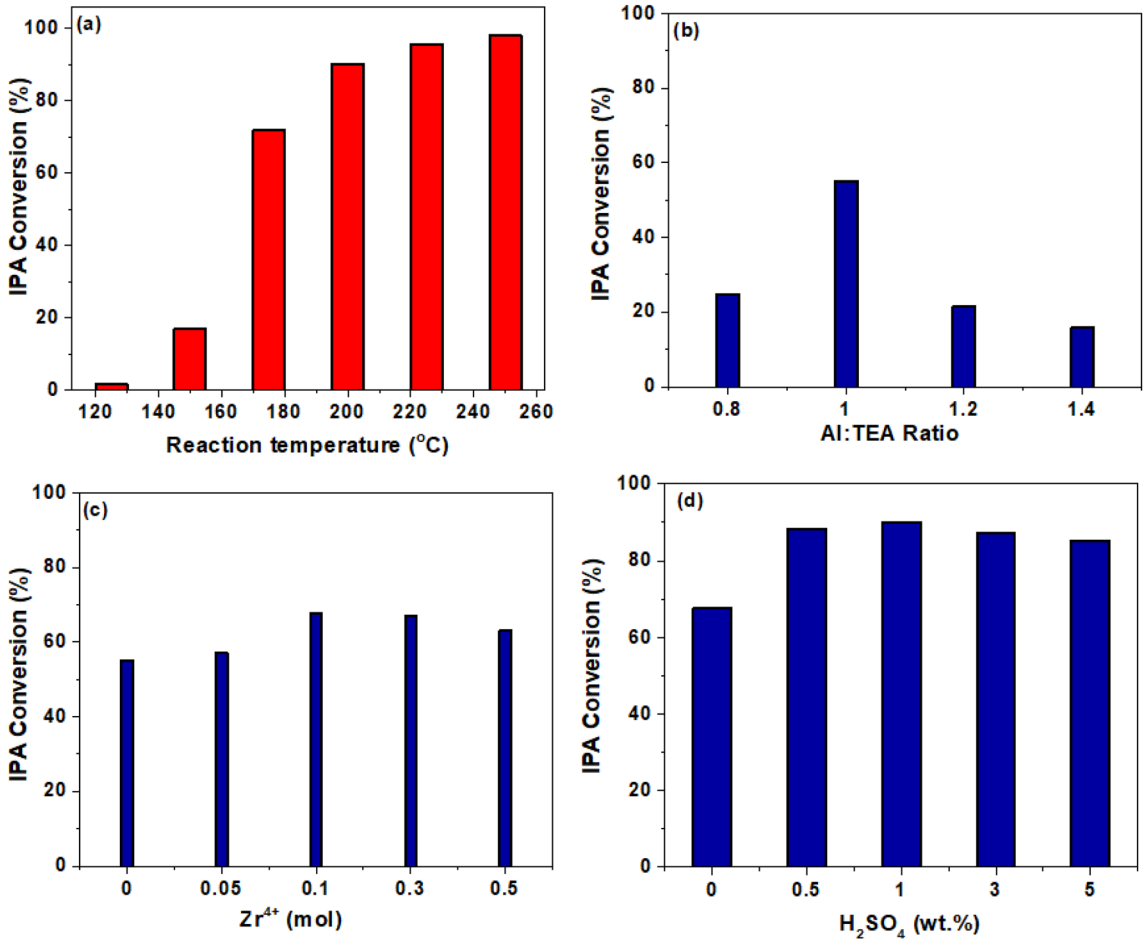

Fig. 6 Catalytic dehydration of isopropanol over, **a** 0.1 zirconium substituted $AlPO_4$-1T modified with 1% H_2SO_4 catalyst calcined at 400 °C, **b** $AlPO_4$-1T with different ratios of TEA catalyst at reaction temperature of 200 °C, **c** Zr^{4+}-incorporated $AlPO_4$-1T catalysts at reaction temperature of 200 °C, and **d** 0.1Zr-$AlPO_4$-1T modified with different percentages of H_2SO_4 at reaction temperature of 200 °C

Incorporation of zirconia into $AlPO_4$-1T matrix (Fig. 6c) developed an incremental increase in IPA conversion, where it was observed that IPA increased from 55 to 68% over the pure and that incorporated with 0.1 mol% Zr^{4+}, respectively. The further increase in Zr^{4+} content resulted in a slight decrease in IPA, reflecting that substitution with 0.1 Zr is the most proper ratio. It was reported that the isomorphous substitution of framework Al^{3+} ions by Zr^{4+} ions in alumiophosphate zeolitic structure resulted in creation of Brønsted and Lewis acidity [39]. At the same reaction temperature, IPA conversion was studied over 0.1Zr-$AlPO_4$-1T catalyst impregnated with different percentages of sulfuric acid and the results were described in Fig. 6d. It indicated that IPA conversion dramatically increases from 68 to 95% over catalyst impregnated with 1% H_2SO_4. The further % of sulfuric acid impregnation gave almost the same acidity with a slight decrease in IPA conversion. This implies that a perceptible change improvement of surface acidity and 100% for propene selectivity was observed. These findings are confirmed by FTIR results where it was pointed out that the intensity of the band related to P–OH bond groups responsible for acidity, are increased with increasing both Zr^{4+} or sulfuric acid impregnation [54, 55].

However, IPA dehydration only evaluated the total acidity, while type and strength of the acidic sites could not be estimated from this reaction. To identify the typology [Lewis (L) and Brønsted (B)] and strength of acidic sites, additional investigations were carried out. It was possible to distinguish between Lewis (L) and Brønsted (B) acid sites using the chemisorption of basic probe molecules, such as pyridine (PY) and dimethyl pyridine (DMPY) [65]. In these procedures, on both Lewis and Brønsted types of acidic sites, pyridine molecules often chemisorb. While steric hindrance of two the methyl groups causes DMPY molecules to chemisorb preferentially on Brønsted acid sites [45, 46].

The poisoning of the acid sites with the basic probes during IPA dehydration over the surface of 1% H_2SO_4–Zr-$AlPO_4$-1T catalyst at 200 °C was investigated,

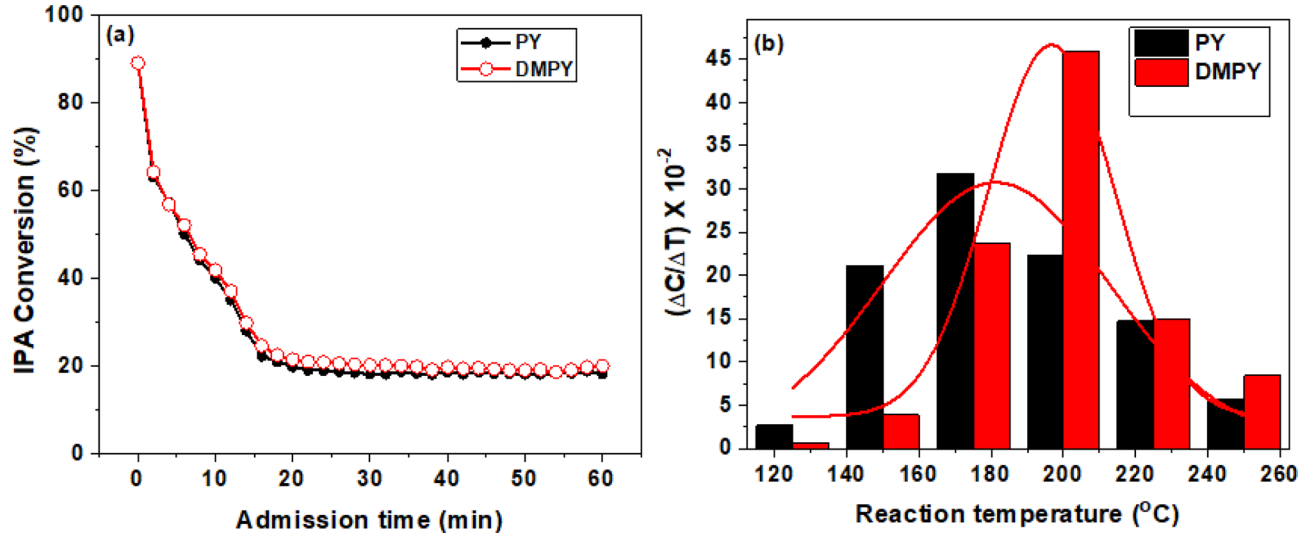

Fig. 7 **a** Impact of PY and DMPY injection times on IPA conversion variation, at 200 °C, over 1% H_2SO_4–Zr-$AlPO_4$-1T catalyst calcined at 400 °C, and **b** desorption of PY and DMPY from the surface of previously saturated 1% H_2SO_4–Zr-$AlPO_4$-1T catalyst calcined at 400 °C

and the data are presented in Fig. 7a. It indicated that the % conversion of IPA dramatically reduces with raising the injection time of vapors of both PY and DMPY to achieve a steady state at 20 min, with IPA conversions of 21 and 22%, respectively. The decrease in IPA conversion is due to the poisoning effect of acidic sites by the basic probs. Furthermore, a difference of about 1% between the two conversions indicates that most of the acid sites are of the Brønsted type [65]. In this context, it was reported that the hydroxyl groups on the P atom (P–OH) are highly acidic than that over Al atom (Al–OH) in Al_2O_3 catalysts indicating that, the Brønsted acidic sites over $AlPO_4$-1T are comfortable for formation of the methoxy groups as an intermediate which eventually interact with methanol molecule to form DME [52, 53].

To measure the acidic site strength, the most active catalyst, 1% H_2SO_4–0.1Zr-$AlPO_4$-1T, was previously saturated with the vapors of the basic probes for about 10 days and tested for IPA decomposition at various reaction temperatures, according to the procedures previously reported [46, 66], and the results are presented in Fig. 7b. It reveals that, most of the probe molecules were left the surface at a temperature range of 175–200 °C, suggesting that the acid sites available on the catalyst surface are of medium strength. Total acidity and strength of the acidic sites were also confirmed by pyridine-TPD [Table 4; Fig. S14 (ESI)]. Results presented in Table 4 indicated the variation in acidity with Zr^{4+} incorporation and sulfuric acid modification is well-matched with the results of IPA conversion (Fig. 6). In addition, most of acid sites are of weak and intermediary strengths. Furthermore, little amounts of strong acidic sites were observed over the catalyst's surfaces.

3.3 Catalytic Activity

Figure 8 presents the results of the experimental procedures to produce DME from methyl alcohol dehydration over catalysts under study. DME was the only product with a selectivity of 100% throughout all activity runs and at all reaction temperatures. All catalysts have an analogous attitude, in which the catalytic activity increases as reaction temperature increases. Figure 8a presents the catalytic activity results for the $AlPO_4$-0.8T, $AlPO_4$-1T, $AlPO_4$-1.2T, and $AlPO_4$-1.4T catalysts calcined at 400 °C in the temperature range of 200–400 °C. It indicates that $AlPO_4$-1T

Table 4 Total acidity and strength of acidic sites

Catalyst	(Sites $g^{-1}_{cat} \times 10^{20}$)			
	Total acidity	Weak (RT–150 °C)	Medium (150–350 °C)	Strong > 350 °C
$AlPO_4$-1T	7.74	4.60	3.01	0.13
0.1Zr-$AlPO_4$-1T	7.88	3.86	3.11	0.91
1% H_2SO_4–Zr-$AlPO_4$-1T	8.54	4.22	3.28	1.04

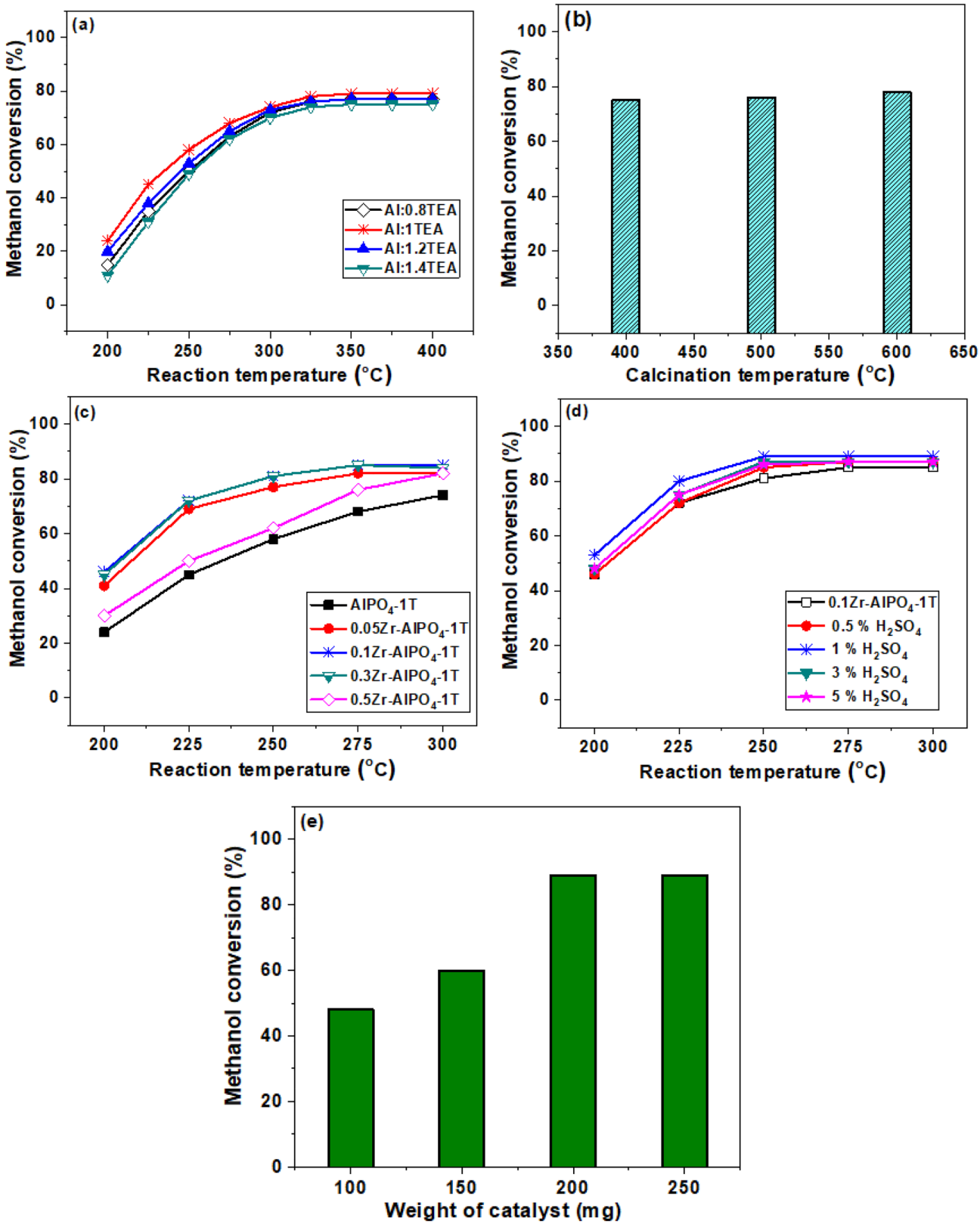

Fig. 8 Catalytic dehydration of methanol into DME over **a** $AlPO_4$-TRI with different ratios of TEA, **b** $AlPO_4$-1 catalyst calcined at different temperatures, **c** Zr-incorporated $AlPO_4$-1T catalysts, **d** 0.1Zr-$AlPO_4$-1T modified with different percentages of H_2SO_4, and **e** different weights of 1% H_2SO_4–Zr-$AlPO_4$-1T catalyst at a reaction temperature of 250 °C

exhibits the highest activity for methanol dehydration, with a conversion of 78% at 300 °C. This behavior may be attributed to the high S_{BET} value exhibited by this catalyst among the other ones (Table 3). Figure 8b shows the effect of calcination temperature on the methanol dehydration activity over $AlPO_4$-1T at the reaction temperature 300 °C. There is no fundamental difference in the % conversion of methanol and % yield of DME upon increasing the calcination temperature up to 600 °C. Only a slight increase in the % conversion not exceeding 3–5% while the selectivity is still 100% to DME. However, such a slight increase cannot be interpreted in terms of the variation in S_{BET} (Table 3) where catalyst calcined at 400 °C possessed higher S_{BET} than that annealed at 600 °C. This increase may be attributed to the slight conversion of the monoclinic phase of $AlPO_4$-1T into the semi-amorphous state [46]. These findings manifested the stability of catalysts with annealing temperatures. In addition, owing to a catalyst calcined at 400 °C having a definite chemical structure (Tridymite), it was chosen for further investigations like Zr^{4+} incorporation, and sulfuric acid modification. Figure 8c shows the influence of the incorporation of zirconia in $AlPO_4$-1T on its activity and selectivity. It indicated that the best ratio for substitution is 0.1, with conversions of 81 and 85% at 250 and 275 °C, respectively. Such results presented the role of Zr^{4+} incorporation in enhancing the catalytic performance of $AlPO_4$-1T where at 250 °C, the methanol conversion greatly enhanced from 58 into 81% on incorporating the $AlPO_4$-1T catalyst with a 0.1 mol% Zr^{4+}. These findings confirmed the role of Zr^{4+} incorporation in enhancing the catalytic conversion of methanol into DME over $AlPO_4$-1T molecular sieves. It was previously reported that, the incorporation of transition metal ions such as Zr^{4+} can create more Brønsted acidity [39] (Fig. 7a). In this context, it was informed that, "the isomorphous substitution of aluminophosphate with poly charged cation greatly enhanced the catalytic activity and selectivity of the final product [67]". In addition, XRD results presented in Fig. 1c revealed that the substitution results in converting the monoclinic phase into a semi-amorphous phase which is accompanied by an observable increase in the S_{BET} values of these catalysts (Table 3). It was found that incorporating $AlPO_4$-1T molecular sieves with 0.1 mol% Zr^{4+} improved the S_{BET} values by 14.2%. Also, this treatment improved the IPA conversion from 55 to 68% (Fig. 6c).

To enhance the catalytic activity, the 0.1Zr-$AlPO_4$-1T was further modified by sulfuric acid and the results are given in Fig. 8d. It shows that, at a reaction temperature of 250 °C, an 89% yield of DME was obtained over 1% H_2SO_4–0.1Zr-$AlPO_4$-1T, which is in consistency with thermodynamic equilibrium conversion. This enhancement in activity agrees with the results presented in Table 3 where treatment of 0.1Zr-$AlPO_4$-1T with 1% H_2SO_4 sulfuric acid resulted in increasing the S_{BET} from 55.3 to 63.3 $m^2\ g^{-1}$. The fluctuation in catalytic activity with changing the ratios of TEA, Zr, and H_2SO_4 is closely related to the alteration in catalyst acidities.

The influence of catalyst weight was also studied over the 1% H_2SO_4–0.1Zr-$AlPO_4$-1T catalyst, as depicted in Fig. 8e. The results showed that, at 250 °C, on increasing the catalyst weight from 100 to 200 mg, a dramatic enhancement was observed where the conversion changed from 48 to 89%. This improvement could be explained by a rise in the weight of the catalyst leading to an increase in the number of active sites. The further increase in catalyst weight, i.e., 250 mg, gave almost the same activity. Accordingly, to remove the mass transfer effect, a weight of 200 mg was used in all catalytic runs.

To shed a light on the activation energy of methanol dehydration, the initial rate of reaction was calculated as previously reported [46] and the results are displayed in Table 5 and Fig. S15 (ESI). Again, we can attribute the variation in catalytic activity among the different catalysts to the variation in activation energy values. In addition, these values are comparable to that previously reported [68, 69].

Figure 9a shows the influence of reactant contact time stated as gas hourly space velocity (GHSV) on the catalytic activity of 1% H_2SO_4–0.1Zr-$AlPO_4$-1T catalyst at 250 °C. It implies that GHSV of 15,000 ml $g^{-1}\ h^{-1}$ gives the maximum conversion of 89%. Upon raising the GHSV from 15,000 to 45,000 ml $g^{-1}\ h^{-1}$, a reduction in the % conversion to reach 55% was noted. Such performance may be ascribed to the low contact time of methyl alcohol molecules on the catalyst surface [46]. The effect of the reactant concentration, as methanol % in the reacting stream, was also examined over 1% H_2SO_4–0.1Zr-$AlPO_4$-1T catalyst at 250 °C and is shown in Fig. 9b. The results revealed that increasing the concentration of methanol resulted in a significant decrease in conversion, while 100% DME selectivity was sustained. Since catalyst reusability and recycling is a great

Table 5 Activation energy values of the prepared catalysts

Catalyst	ΔE_a (kJ mol^{-1})
$AlPO_4$-1T	51.0
0.8T	86.0
1.2T	52.0
1.4T	119.1
0.05Zr	23.0
0.1Zr	22.9
0.3Zr	24.8
0.5Zr	28.4
0.5% H_2SO_4	23.4
1% H_2SO_4	20.1
3% H_2SO_4	22.5
5% H_2SO_4	24.9

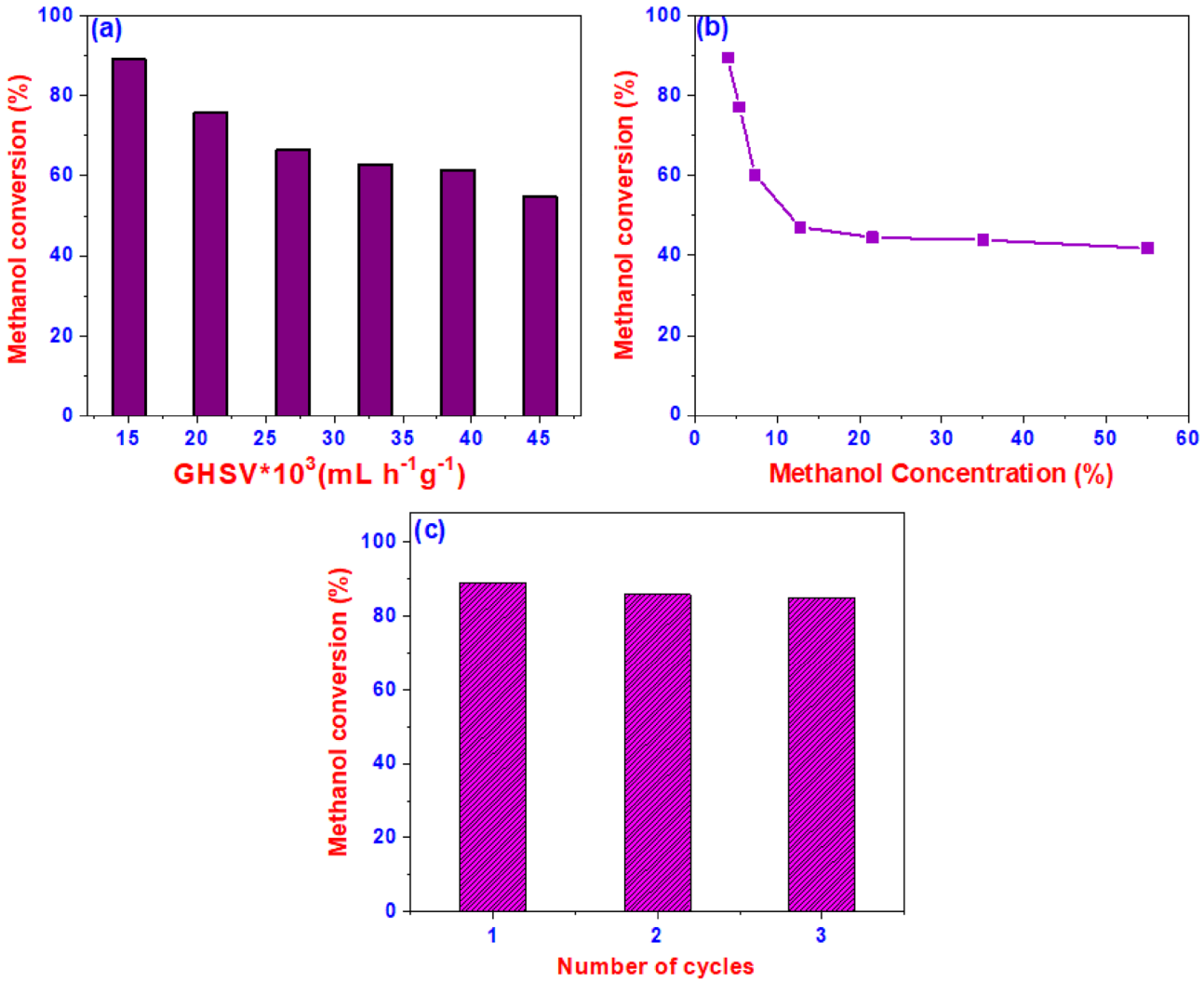

Fig. 9 Effect of **a** GHSV, **b** % of methanol over 1% H_2SO_4–Zr-$AlPO_4$-1T catalyst calcined at 400 °C (at a reaction temperature of 250 °C and atmospheric pressure), and **c** reusability of 1% H_2SO_4–Zr-$AlPO_4$-1T catalyst towards methanol dehydration into DME at 250 °C

issue especially in industrial catalysis, regeneration of 1% H_2SO_4–0.1Zr-$AlPO_4$-1T was studied for three cycles. After the first catalytic run, the spent catalyst was collected and calcined in the muffle furnace at 400 °C for 3 h and subject to methanol dehydration under similar conditions of the fresh catalyst. The same procedures were repeated for second and third cycles, and the results are presented in Fig. 9c. The catalyst regeneration process comprises that the regenerated calcined catalyst can be used for many cycles without any deactivation and produces a similar yield for the first cycle at 250 °C with a little decrease not exceeding 3%. The stability of the catalyst was also examined by following up the reaction over the catalyst surface for a period of 120 h at 250 °C (Fig. S16). It shows that the catalyst is still efficient towards the dehydration reaction, with almost the same activity and 100% selectivity. These findings confirmed that, the number and nature of acidic sites remained unchanged under the investigated conditions [70]. TGA of the spent catalyst was carried in a temperature range of 25–600 °C in air atmosphere and the obtained results are presented in Fig. S17. It shows that only a 1.6% weight loss was observed on heating the spent catalyst up to 600 °C. Actually, it is a neglectable value and confirmed the absence of any coke formation. Also, this result can safely clearly explain the dramatic long-term stability and recyclability of the catalyst under study. Finally, a comparison was made between the catalytic behavior of the 1% H_2SO_4–0.1Zr-$AlPO_4$-1T catalyst provided in this investigation and that reported in the literature, and the results are shown in Table 6. Inspection of these results revealed that the catalyst 1% H_2SO_4–0.1Zr-$AlPO_4$-1T possessed the highest activity at relatively low reaction temperature at 250 °C, with conversion of 89% and selectivity 100%. In addition, the catalysts offer a long-term stability for the reaction for 120 h with approximately the same activity and selectivity.

Table 6 The catalytic performance of 1% H_2SO_4/0.1Zr-$AlPO_4$-TRI catalyst towards methanol dehydration into DME and that previously reported catalysts

Catalyst	Temperature (°C)	Methanol conversion (%)	DME selectivity (%)	References
AlPO-5	350	81.0	99.6	[40]
AlPO-11	350	81.4	99.9	[40]
AlPO-41	350	82.4	99.9	[40]
SAPO-5	250	85	68.1	[40]
SAPO-11	250	84.1	100	[40]
SAPO-41	250	81.3	82.1	[40]
Na-modified H-ZSM-5 $NaNO_3$	270	~83	100	[71]
NaH-ZSM-5 $NaNO_3$	250	~60	100	[72]
Na-modified H-ZSM-5 $NaNO_3$	300	98	100	[73]
H-ZSM-5/MCM-41 NaOH + CTAB	220	~90	100	[74]
HMS no Al insertion, DDA surfactant	300	10	NA	[75]
Al-HMS-5 Si/Al = 5, DDA surfactant	300	91.2	94.1	[75]
Al-HMS-10 Si/Al = 10, DDA surfactant	300	89	100	[75]
Al-HMS-20 Si/Al = 20, DDA surfactant	325	20	100	[75]
Al-HMS-35 Si/Al = 35, DDA surfactant	375	16	100	[75]
SAPO-46	350	80	93	[76]
1% H_2SO_4/0.1Zr-$AlPO_4$-1 T	250	89	100	This work

4 Conclusions

In this study, pure and Zr^{4+}-incorporated $AlPO_4$-TRI molecular sieve nanocatalysts were successfully prepared and tested for the selective production of DME. An 89% conversion of methanol and 100% selectivity into DME was obtained at 250 °C over the sulfuric acid modified Zr-incorporated $AlPO_4$-TRI. The texture of these catalysts exhibited micropores with narrow width. Catalysts generated Brønsted acid sites of weak and medium strengths. Activity was well correlated with the catalyst acidity and activation energy. Catalysts could be reused three times with similar activity and selectivity. In addition, catalyst offered a dramatic stability towards methanol conversion into DME for long period of time of 120 h. All these benefits encourage the use of sulfuric acid modified Zr-incorporated $AlPO_4$-TRI as sustainable and promising nancatalysts for producing DME.

Supplementary Information The online version contains supplementary material available at https://doi.org/10.1007/s10562-023-04370-7.

Acknowledgements The author would thank the Institutional Review Board (IRB) of the Faculty of Science at Assiut University, Egypt for the financial support.

Funding Open access funding provided by The Science, Technology & Innovation Funding Authority (STDF) in cooperation with The Egyptian Knowledge Bank (EKB).

Declarations

Conflict of interest Authors declare no conflict of interest.

References

1. Sun J, Yang G, Yoneyama Y, Tsubaki N (2014) Catalysis chemistry of dimethyl ether synthesis. ACS Catal 4:3346–3356
2. Arcoumanis C, Bae C, Crookes R et al (2008) The potential of di-methyl ether (DME) as an alternative fuel for compression–ignition engines: a review. Fuel 87(7):1014–1030
3. Park SH, Lee CS (2014) Applicability of dimethyl ether (DME) in a compression ignition engine as an alternative fuel. Energy Convers Manag 86:848–863
4. Wei SP, Li C (2023) Design and optimization of spiral heated tubular dimethyl ether (DME) steam reforming reactor. Int J Hydrog Energy 48:2231–2246. https://doi.org/10.1016/J.IJHYDENE.2022.09.295
5. Torres-Liñ J, García-Rollán M, Rosas JM et al (2021) Deactivation of a biomass-derived zirconium-doped phosphorus-containing carbon catalyst in the production of dimethyl ether from methanol dehydration. Energy Fuels 35:17225–17240. https://doi.org/10.1021/acs.energyfuels.1c01721
6. Goda MN, Abdelhamid HN, Said AEAA (2020) Zirconium oxide sulfate-carbon ($ZrOSO_4$@C) derived from carbonized UiO-66 for selective production of dimethyl ether. ACS Appl

Mater Interfaces 12:646–653. https://doi.org/10.1021/acsami.9b17520
7. Armenta MA, Maytorena VM, Flores-Sánchez LA et al (2020) Dimethyl ether production via methanol dehydration using Fe_3O_4 and CuO over γ–χ-Al_2O_3 nanocatalysts. Fuel 280:118545. https://doi.org/10.1016/j.fuel.2020.118545
8. Alharbi W, Kozhevnikova EF, Kozhevnikov IV (2015) Dehydration of methanol to dimethyl ether over heteropoly acid catalysts: the relationship between reaction rate and catalyst acid strength. ACS Catal 5:7186–7193. https://doi.org/10.1021/acscatal.5b01911
9. Saravanan K, Ham H, Tsubaki N, Bae JW (2017) Recent progress for direct synthesis of dimethyl ether from syngas on the heterogeneous bifunctional hybrid catalysts. Appl Catal B 217:494–522
10. Kriprasertkul W, Witoon T, Kim-Lohsoontorn P (2022) Dimethyl ether (DME) synthesis from CO_2 and H_2 through ethanol-assisted methanol synthesis and methanol dehydration. Int J Hydrog Energy 47:33338–33351. https://doi.org/10.1016/J.IJHYDENE.2022.07.212
11. Bonura G, Todaro S, Frusteri L et al (2021) Inside the reaction mechanism of direct CO_2 conversion to DME over zeolite-based hybrid catalysts. Appl Catal B 294:120255. https://doi.org/10.1016/J.APCATB.2021.120255
12. Takeguchi T, Yanagisawa KI, Inui T, Inoue M (2000) Effect of the property of solid acid upon syngas-to-dimethyl ether conversion on the hybrid catalysts composed of Cu–Zn–Ga and solid acids. Appl Catal A 192:201–209. https://doi.org/10.1016/S0926-860X(99)00343-9
13. Raoof F, Taghizadeh M, Eliassi A, Yaripour F (2008) Effects of temperature and feed composition on catalytic dehydration of methanol to dimethyl ether over γ-alumina. Fuel 87:2967–2971. https://doi.org/10.1016/j.fuel.2008.03.025
14. Rownaghi AA, Rezaei F, Stante M, Hedlund J (2012) Selective dehydration of methanol to dimethyl ether on ZSM-5 nanocrystals. Appl Catal B 119–120:56–61. https://doi.org/10.1016/j.apcatb.2012.02.017
15. Zeng L, Wang Y, Mou J et al (2020) Promoted catalytic behavior over γ-Al_2O_3 composited with ZSM-5 for crude methanol conversion to dimethyl ether. Int J Hydrog Energy 45:16500–16508. https://doi.org/10.1016/j.ijhydene.2020.04.115
16. Magzoub F, Li X, Lawson S et al (2020) 3D-printed HZSM-5 and 3D-HZM5@SAPO-34 structured monoliths with controlled acidity and porosity for conversion of methanol to dimethyl either. Fuel 280:118628. https://doi.org/10.1016/j.fuel.2020.118628
17. Vishwanathan V, Jun KW, Kim JW, Roh HS (2004) Vapour phase dehydration of crude methanol to dimethyl ether over Na-modified H-ZSM-5 catalysts. Appl Catal A 276:251–255. https://doi.org/10.1016/j.apcata.2004.08.011
18. Boon J, van Kampen J, Hoogendoorn R et al (2019) Reversible deactivation of Γ-alumina by steam in the gas-phase dehydration of methanol to dimethyl ether. Catal Commun 119:22–27. https://doi.org/10.1016/j.catcom.2018.10.008
19. Al-Faze R, Finch A, Kozhevnikova EF, Kozhevnikov IV (2020) Dehydration of methanol and ethanol over silica-supported heteropoly acids in the gas phase: surface-type versus bulk-type catalysis mechanism. Appl Catal A 597:117549. https://doi.org/10.1016/j.apcata.2020.117549
20. Schnee J, Eggermont A, Gaigneaux EM (2017) Boron nitride: a support for highly active hetero polyacids in the methanol-to-DME reaction. ACS Catal 7:4011–4017. https://doi.org/10.1021/acscatal.7b00808
21. Barbarossa V, Viscardi R, Maestri G et al (2019) Sulfonated catalysts for methanol dehydration to dimethyl ether (DME). Mater Res Bull 113:64–69. https://doi.org/10.1016/j.materresbull.2019.01.018
22. Said AEAA, Goda MN, Kassem MA (2020) Promotional effect of B_2O_3, WO_3 and ZrO_2 on the structural, textural and catalytic properties of $FePO_4$ catalyst towards the selective dehydration of methanol into dimethyl ether. Catal Lett 150:1714–1728. https://doi.org/10.1007/s10562-019-03081-2
23. Lima SH, Forrester AMS, Palacio LA, Faro AC (2014) Niobia-alumina as methanol dehydration component in mixed catalyst systems for dimethyl ether production from syngas. Appl Catal A 488:19–27. https://doi.org/10.1016/j.apcata.2014.09.022
24. Said AEAA, Abd El-Wahab MM, El-Aal MA (2014) The catalytic performance of sulfated zirconia in the dehydration of methanol to dimethyl ether. J Mol Catal A 394:40–47. https://doi.org/10.1016/j.molcata.2014.06.041
25. Chen Z, Li X, Xu Y et al (2018) Fabrication of nano-sized SAPO-11 crystals with enhanced dehydration of methanol to dimethyl ether. Catal Commun 103:1–4. https://doi.org/10.1016/j.catcom.2017.09.002
26. Moradi GR, Yaripour F, Vale-Sheyda P (2010) Catalytic dehydration of methanol to dimethyl ether over mordenite catalysts. Fuel Process Technol 91:461–468. https://doi.org/10.1016/j.fuproc.2009.12.005
27. Akarmazyan SS, Panagiotopoulou P, Kambolis A et al (2014) Methanol dehydration to dimethylether over Al_2O_3 catalysts. Appl Catal B 145:136–148. https://doi.org/10.1016/j.apcatb.2012.11.043
28. Cara C, Secci F, Lai S et al (2022) On the design of mesostructured acidic catalysts for the one-pot dimethyl ether production from CO_2. J CO2 Util 62:102066. https://doi.org/10.1016/J.JCOU.2022.102066
29. Fu Y, Hong T, Chen J et al (2005) Surface acidity and the dehydration of methanol to dimethyl ether. Thermochim Acta 434:22–26. https://doi.org/10.1016/J.TCA.2004.12.023
30. Wan Y, Williams CD, Duke CVA, Cox JJ (2000) Systematic studies on the effect of water content on the synthesis, crystallisation, conversion and morphology of $AlPO_4$-5 molecular sieve. J Mater Chem 10:2857–2862. https://doi.org/10.1039/b006127l
31. Said S, Aman D, Riad M, Mikhail S (2020) MoZn/$AlPO_4$-5 zeolite: preparation, structural characterization and catalytic dehydration of ethanol. J Solid State Chem 287:121335. https://doi.org/10.1016/j.jssc.2020.121335
32. Dedecek J, Balgová V, Pashkova V et al (2012) Synthesis of ZSM-5 zeolites with defined distribution of Al atoms in the framework and multinuclear MAS NMR analysis of the control of Al distribution. Chem Mater 24:3231–3239
33. Liang Y, Jacobson A, Letters JR-AM (2020) U (2021) Strontium ions function as both an accelerant and structure-directing agent of chabazite crystallization. ACS Mater Lett 3:187–192
34. Prakash AM, Chilukuri SVV, Bagwe RP et al (1996) Silicoaluminophosphate molecular sieves SAPO-11, SAPO-31 and SAPO-41: synthesis, characterization and alkylation of toluene with methanol. Microporous Mater 6:89–97. https://doi.org/10.1016/0927-6513(95)00091-7
35. Tanabe K, Yamaguchi T (1994) Acid–base bifunctional catalysis by ZrO_2 and its mixed oxides. Catal Today 20:185–197. https://doi.org/10.1016/0920-5861(94)80002-2
36. Yamaguchi T (1994) Application of ZrO_2 as a catalyst and a catalyst support. Catal Today 20:199–217. https://doi.org/10.1016/0920-5861(94)80003-0
37. Sajan CP, Suresh Kumar BV, Naik A (2016) Comparative study of hydrothermally synthesized $AlPO_4$-5, activated carbon, and the combination of activated carbon and $AlPO_4$-5 filters in the treatment of wastewater and industrial effluent. Water Conserv Sci Eng 1:177–195. https://doi.org/10.1007/s41101-016-0012-0
38. Mortén M, Cordero-Lanzac T, Cnudde P et al (2021) Acidity effect on benzene methylation kinetics over substituted

H-MeAlPO-5 catalysts. J Catal 404:594–606. https://doi.org/10.1016/j.jcat.2021.11.002
39. Dongare MK, Sabde DP, Shaikh RA et al (1999) Synthesis, characterization and catalytic properties of ZrAPO-5. Catal Today 49:267–276. https://doi.org/10.1016/S0920-5861(98)00433-7
40. Dai W, Kong W, Wu G et al (2011) Catalytic dehydration of methanol to dimethyl ether over aluminophosphate and silicoaluminophosphate molecular sieves. Catal Commun 12:535–538
41. Basina G, AlShami D, Polychronopoulou K et al (2018) Hierarchical $AlPO_4$-5 and SAPO-5 microporous molecular sieves with mesoporous connectivity for water sorption applications. Surf Coat Technol 353:378–386. https://doi.org/10.1016/j.surfcoat.2018.08.083
42. Osman AI, Abu-Dahrieh JK, Rooney DW et al (2012) Effect of precursor on the performance of alumina for the dehydration of methanol to dimethyl ether. Appl Catal B 127:307–315. https://doi.org/10.1016/j.apcatb.2012.08.033
43. Goda MN, Said AEAA, Abdelhamid HN (2021) Highly selective dehydration of methanol over metal–organic frameworks (MOFs)-derived ZnO@carbon. J Environ Chem Eng 9:106336. https://doi.org/10.1016/J.JECE.2021.106336
44. Said AEAA, El-Wahab MMMA, Alian AM (2016) Selective oxidation of methanol to formaldehyde over active molybdenum oxide supported on hydroxyapatite catalysts. Catal Lett 146:82–90. https://doi.org/10.1007/s10562-015-1624-2
45. Khalil KMS, Elhamdy WA, Goda MN, Said AE-AA (2021) Biomass derived P-containing activated carbon as a novel green catalyst/support for methanol conversion to dimethyl ether alternative fuel. J Environ Chem Eng 9:106572. https://doi.org/10.1016/J.JECE.2021.106572
46. Said AEA, Goda MN, Shaban AA (2021) The catalytic performance of ultrasonically prepared $AlPO_4$ nanocatalysts for the selective production of dimethyl ether from methanol. Catal Lett 152:821–837. https://doi.org/10.1007/s10562-021-03664-y
47. Slavinskaya EM, Gulyaev RV, Zadesenets AV et al (2015) Low-temperature CO oxidation by Pd/CeO_2 catalysts synthesized using the coprecipitation method. Appl Catal B 166–167:91–103. https://doi.org/10.1016/J.APCATB.2014.11.015
48. Graetsch HA (2002) Monoclinic $AlPO_4$-5 tridymite at 473 and 463 K from X-ray powder data. Acta Crystallogr C 58:i18–i20
49. Min HK, Kim YW, Kim C et al (2022) Phase transformation of ZrO_2 by Si incorporation and catalytic activity for isopropyl alcohol dehydration and dehydrogenation. Chem Eng J 428:131766. https://doi.org/10.1016/j.cej.2021.131766
50. Chakrabortty D, Ganguli JN, Satyanarayana CVV (2011) Incorporation of zirconium in medium-pore aluminophosphate molecular sieves with AFO framework. Microporous Mesoporous Mater 137:65–71. https://doi.org/10.1016/j.micromeso.2010.08.022
51. Miller FA (1964) Chemical technology: chemical applications of infrared spectroscopy. C. N. R. Rao. Academic, New York, 1963. xiv + 683 pp. Illus. $19.50. Science (80-) 144:1441–1441. https://doi.org/10.1126/science.144.3625.1441.a
52. Lertjiamratn K, Praserthdam P, Arai M, Panpranot J (2010) Modification of acid properties and catalytic properties of $AlPO_4$ by hydrothermal pretreatment for methanol dehydration to dimethyl ether. Appl Catal A 378:119–123. https://doi.org/10.1016/j.apcata.2010.02.013
53. Liu H, Kianfar E (2021) Investigation the synthesis of nano-SAPO-34 catalyst prepared by different templates for MTO process. Catal Lett 151:787–802. https://doi.org/10.1007/s10562-020-03333-6
54. Moffat JB, Vetrivel R, Viswanathan B (1985) A model cluster study of the acid–base properties of phosphate catalysts. J Mol Catal 30:171–180. https://doi.org/10.1016/0304-5102(85)80025-0
55. Kianfar E (2019) Ethylene to propylene over zeolite ZSM-5: improved catalyst performance by treatment with CuO. Russ J Appl Chem 92:933–939. https://doi.org/10.1134/S1070427219070085
56. Kianfar E (2021) Investigation of the effect of crystallization temperature and time in synthesis of SAPO-34 catalyst for the production of light olefins. Pet Chem 61:527–537. https://doi.org/10.1134/S0965544121050030
57. Murayama N, Okajima N et al (2006) Hydrothermal synthesis of $AlPO_4$-5 type zeolitic materials by using aluminum dross as a raw material. J Eur Ceram Soc 26:459–462
58. Zhang S, Cui M, Zhang Y et al (2017) Study on the oxidation transformation of hexamethyleneimine in a confined region of zeolites. Microporous Mesoporous Mater 244:158–163. https://doi.org/10.1016/j.micromeso.2017.02.066
59. Ganguli JN, Chakrabortty D, Satyanarayana CVV (2008) Incorporation of zirconium in medium-pore aluminophosphate molecular sieves with AEL framework. Microporous Mesoporous Mater 108:223–229. https://doi.org/10.1016/j.micromeso.2007.03.044
60. Brunauer S, Emmett PH, Teller E (1938) Adsorption of gases in multimolecular layers. J Am Chem Soc 60:309–319. https://doi.org/10.1021/ja01269a023
61. Fukumori Y, Takeuchi H, Ando Y (2018) Structural control of nanoparticles. In: Nanoparticle technology handbook. Elsevier, Amsterdam, pp 49–107
62. Lippens BC, de Boer JH (1965) Studies on pore systems in catalysts. V. The t method. J Catal 4:319–323. https://doi.org/10.1016/0021-9517(65)90307-6
63. Said AE-AA, Goda MN (2018) Superior catalytic performance of $CaMoO_4$ catalyst in direct dehydrogenation of methanol into anhydrous formaldehyde. Chem Phys Lett 703:44–51
64. Hočevar S, Batista J, Kaučič V (1993) Acidity and catalytic activity of MeAPSO-44 (Me = Co, Mn, Cr, Zn, Mg), SAPO-44, $AlPO_4$-5, and $AlPO_4$-14 molecular sieves in methanol dehydration. J Catal 139:351–361. https://doi.org/10.1006/jcat.1993.1030
65. Mohd Ekhsan J, Lee SL, Nur H (2014) Niobium oxide and phosphoric acid impregnated silica–titania as oxidative-acidic bifunctional catalyst. Appl Catal A 471:142–148. https://doi.org/10.1016/j.apcata.2013.11.041
66. Said AEAA, Heikal MTS, Goda MN (2019) Characterization and catalytic performance of basaltic dust as an efficient catalyst in the liquid-phase esterification of acetic acid with *n*-butanol. J Chin Chem Soc 66:725–733. https://doi.org/10.1002/jccs.201800397
67. Spivey JJ (1991) Review: Dehydration catalysts for the methanol/dimethyl ether reaction. Chem Eng Commun 110:123–142. https://doi.org/10.1080/00986449108939946
68. Tavan Y, Nikou MRK, Shariati A (2014) Effect of the P/Al ratio on the performance of modified HZSM-5 for methanol dehydration reaction. J Ind Eng Chem 20:668–673. https://doi.org/10.1016/j.jiec.2013.05.031
69. Hosseininejad S, Afacan A, Hayes RE (2012) Catalytic and kinetic study of methanol dehydration to dimethyl ether. Chem Eng Res Des 90:825–833. https://doi.org/10.1016/j.cherd.2011.10.007
70. Kanjanasoontorn N, Permsirivanich T, Numpilai T et al (2016) Structure–activity relationships of hierarchical meso–macroporous alumina supported copper catalysts for CO_2 hydrogenation: effects of calcination temperature of alumina support. Catal Lett 146:1943–1955. https://doi.org/10.1007/S10562-016-1849-8/FIGURES/13
71. Vishwanathan V, Jun K, Kim J et al (2004) Vapour phase dehydration of crude methanol to dimethyl ether over Na-modified H-ZSM-5 catalysts. Appl Catal A 276:251–255
72. Jiang S, Hwang J-S, Jin T et al (2004) Dehydration of methanol to dimethyl ether over ZSM-5 zeolite. Bull Korean Chem Soc 25:185–189

73. Hassanpour S, Yaripour F, Taghizadeh M (2010) Performance of modified H-ZSM-5 zeolite for dehydration of methanol to dimethyl ether. Fuel Process Technol 91:1212–1221. https://doi.org/10.1016/j.fuproc.2010.03.035
74. Sang Y, Liu H, He S et al (2013) Catalytic performance of hierarchical H-ZSM-5/MCM-41 for methanol dehydration to dimethyl ether. J Energy Chem 22:769–777. https://doi.org/10.1016/S2095-4956(13)60102-3
75. Sabour B, Peyrovi MH, Hamoule T, Rashidzadeh M (2014) Catalytic dehydration of methanol to dimethyl ether (DME) over Al-HMS catalysts. J Ind Eng Chem 20:222–227. https://doi.org/10.1016/j.jiec.2013.03.044
76. Kong W, Dai W, Li N et al (2009) A one-step route to SAPO-46 using H_3PO_3-containing gel and its application as the catalyst for methanol dehydration. J Mol Catal A 308:127–133. https://doi.org/10.1016/j.molcata.2009.03.036